Jpn. J. Appl. Phys. Vol. 36 (1997) pp. 6237–6243
Part 1, No. 10, October 1997

Optical Constants of ZnO

Hisashi YOSHIKAWA and Sadao ADACHI
Department of Electronic Engineering, Faculty of Engineering, Gunma University, Kiryu, Gunma 376, Japan

(Received June 16, 1997; accepted for publication July 16, 1997)

The complex dielectric functions, $\varepsilon(E) = \varepsilon_1(E) + i\varepsilon_2(E)$, of ZnO have been measured by spectroscopic ellipsometry (SE) in the photon-energy range between 1.5 and 5.0 eV at room temperature. The SE measurements are carried out on the surface parallel to the optic axis c, which allows the determination of the optical constants for light polarized perpendicular ($\boldsymbol{E} \perp c$) and parallel to the c-axis ($\boldsymbol{E} /\!/ c$). The measured SE spectra show the exciton peaks at ~3.4 eV (E_0 edge). These $\varepsilon(E)$ spectra are analyzed on the basis of a simplified model of the interband transitions. Excellent agreement is achieved between the calculated and experimental results over the entire range of photon energies. Dielectric-function-related optical constants, such as the complex refractive index $n^*(E) = n(E) + ik(E)$, absorption coefficient $\alpha(E)$ and normal-incidence reflectivity $R(E)$, of ZnO have also been reported.

KEYWORDS: ZnO, optical constant, dielectric function, refractive index, optical absorption, spectroscopic ellipsometry

1. Introduction

Zinc oxide (ZnO) is a member of the II-VI semiconducting compounds and has a wide band gap, ~3.4 eV at 300 K.[1] It has been used extensively as a photoconducting and fluorescent material, being effective in the visible-to-ultraviolet spectral region. The excellent optical, piezoelectric and acousto-optic properties of ZnO film also make it possible to fabricate solar cell windows,[2] gas sensors,[3] surface acoustic wave devices[4] and integrated acousto-optic devices.[5]

Accurate knowledge of the refractive index and the absorption coefficient of semiconductors is indispensable for the design and analysis of various optical and optoelectronic devices. Note that ZnO crystallizes in the wurtzite structure [space group = $P6_3mc$ (C_{6v}^4)]. The material is thus optically anisotropic (uniaxial). Although there have been many reports on the optical constants of ZnO,[6–18] currently available data in the visible-to-ultraviolet region is less than adequate.

Spectroscopic ellipsometry (SE) is an advantageous technique to investigate the optical constants of semiconductors, in particular, for determining the complex dielectric function $\varepsilon(E) = \varepsilon_1(E) + i\varepsilon_2(E)$. On-line digitization of the data permits the fast and efficient analysis of the structure observed in the $\varepsilon(E)$ spectra in terms of theoretical line shapes for interband critical points (CPs).[19] While most of the SE works have been confined to optically isotropic materials,[20] the usefulness of this technique in the study of anisotropic systems has also been demonstrated (*e.g.*, GaSe,[21] $GeSe_2$[22] GeS,[23,24] CdSe,[25,26] SnSe,[27] α-Al_2O_3[28] and CdS[29]).

In this paper we present the dielectric-function spectra ($\varepsilon = \varepsilon_1 + i\varepsilon_2$) of ZnO for light polarized perpendicular ($\boldsymbol{E} \perp c$) and parallel to the c-axis ($\boldsymbol{E} /\!/ c$) measured by SE in the infrared-near-ultraviolet region (1.5–5.0 eV) at room temperature. It is of both technical and scientific interest to obtain the analytical expression for the optical constants of semiconductors. Therefore, we model our measured $\varepsilon(E)$ spectra using a simplified model of the interband transitions. The model includes the lowest-direct gap E_0 as the main dispersion mechanism. Dielectric-function-related optical constants, such as the complex refractive index, $n^*(E) = n(E) + ik(E)$, absorption coefficient $\alpha(E)$ and normal-incidence reflectivity $R(E)$, are also presented.

2. Theoretical Model

The fundamental absorption edge of ZnO corresponds to the direct transition from the highest valence band to the lowest conduction band at the Γ point ($\boldsymbol{k} = 0$). Figure 1 shows a schematic of the conduction and valence band structures at the Γ point of the zinc-blende (cubic) and wurtzite (hexagonal) crystals. In the hexagonal lattice, the conduction band is s-like, having Γ_7 symmetry. The valence band is p-like, splitting into three doubly degenerate bands with quantum numbers $J_z = 1/2$ (Γ_7), $3/2$ (Γ_9) and $1/2$ (Γ_7) due to the spin-orbit and crystal field interactions. For convenience, the denotations A, B and C are used for these three valence bands. Note that in CdSe and CdS the A valence band has Γ_9 symmetry with $J_z = 3/2$, while B and C have Γ_7 symmetry with $J_z = 1/2$.[26,29] In the cubic lattice, the p-like valence band is split due to the spin-orbit interaction into a fourfold degenerate Γ_8 state and a twofold degenerate Γ_7 state (see Fig. 1).

The polarization vectors $\boldsymbol{E} \perp c$ and $\boldsymbol{E} /\!/ c$ in the hexagonal lattice (C_{6v}^4) belong to the Γ_5 and Γ_1 symmetries, respectively.[30] The direct products between the conduc-

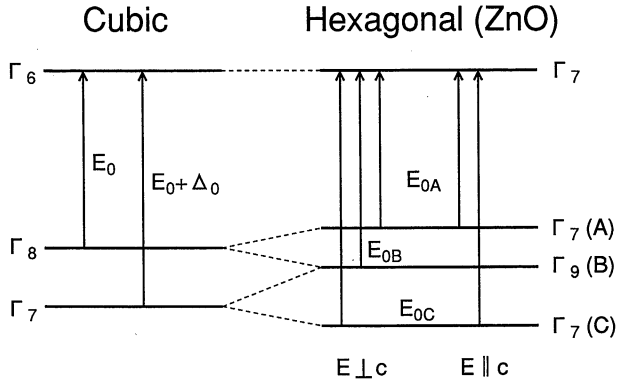

Fig. 1. Energy gaps at the Γ point of the zinc-blende (cubic) and wurtzite (hexagonal) lattices. Note that the E_{0B} transitions are forbidden for $\boldsymbol{E} /\!/ c$.

tion and valence band states can be given by

$$\Gamma_7^v(A) \rightarrow \Gamma_7^c : \ \Gamma_7 \times \Gamma_7 = \Gamma_1 + \Gamma_2 + \Gamma_5, \quad (1.a)$$

$$\Gamma_9^v(B) \rightarrow \Gamma_7^c : \ \Gamma_9 \times \Gamma_7 = \Gamma_5 + \Gamma_6, \quad (1.b)$$

$$\Gamma_7^v(C) \rightarrow \Gamma_7^c : \ \Gamma_7 \times \Gamma_7 = \Gamma_1 + \Gamma_2 + \Gamma_5. \quad (1.c)$$

The direct product $\Gamma_7 \times \Gamma_7$ thus contains the representations for both $\boldsymbol{E} \perp c$ (Γ_5) and $\boldsymbol{E} /\!/ c$ (Γ_1), but $\Gamma_9 \times \Gamma_7$ contains only the representation for $\boldsymbol{E} \perp c$ (Γ_5). This means that for $\boldsymbol{E} /\!/ c$ the optical transitions between the B valence and conduction bands are forbidden while all the optical transitions are possible for $\boldsymbol{E} \perp c$ (see Fig. 1).

The optical constants in the interband transition region of the crystalline materials depend fundamentally on the electronic energy-band structure of the materials. The E_0 gaps in the hexagonal crystals are of the three-dimensional (3D) M_0 CP. Assuming the conduction and valence bands are parabolic and using the Kramers–Kronig (KK) transformation, we obtain the contribution of these gaps to $\varepsilon(E)$:[31]

$$\varepsilon(E) = \sum_{\alpha=A,B,C} A_{0\alpha} E_{0\alpha}^{-1.5} f(\chi_{0\alpha}), \quad (2)$$

with

$$A_{0\alpha} = \frac{4}{3}\left(\frac{3}{2}\mu_{0\alpha}\right)^{1.5} P_{0\alpha}^2, \quad (3)$$

$$f(\chi_{0\alpha}) = \chi_{0\alpha}^{-2}[2 - (1+\chi_{0\alpha})^{1/2} - (1-\chi_{0\alpha})^{1/2}], \quad (4)$$

$$\chi_{0\alpha} = (E + i\Gamma)/E_{0\alpha}. \quad (5)$$

In eqs. (2)–(5), $\mu_{0\alpha}$ is the combined density-of-states mass, $P_{0\alpha}^2$ is the squared momentum-matrix element, Γ is the broadening energy of the $E_{0\alpha}$ gap and α (= A, B, C) denotes the $\Gamma_7(A) \rightarrow \Gamma_7$, $\Gamma_9(B) \rightarrow \Gamma_7$ and $\Gamma_7(C) \rightarrow \Gamma_7$ transitions, respectively.

It is well known that the excitonic interaction in the neighborhood of the lowest-direct band edge of semiconductors dramatically changes the optical spectra.[32] The excitonic transitions play an important role in the fundamental optical process, since the Coulomb interaction is always present between the electrons and the holes. The hydrogenic effective-mass equation provides the solutions of the discrete and the continuum parts of the exciton states.[32] The discrete series of the exciton states at the $E_{0\alpha}$ gap can be simply written, with the Lorentzian line shape, as[31]

$$\varepsilon(E) = \sum_{\alpha=A,B,C} \sum_{n=1}^{\infty} \frac{A_{0\alpha}^{n\alpha}}{E_{x0}^{n\alpha} - E - i\Gamma}, \quad (6)$$

where $A_{0x}^{n\alpha}$ is the discrete-exciton strength parameter and $E_{x0}^{n\alpha}$ is the discrete-exciton energy given by

$$E_{x0}^{n\alpha} = E_{0\alpha} - \frac{G_{0\alpha}^{3D}}{n^2}. \quad (7)$$

In eq. (7) $G_{0\alpha}^{3D}$ is the 3D-exciton Rydberg energy. The 3D-exciton strength parameter $A_{0x}^{n\alpha}$ is proportional to the envelope function ($|\phi_{n\alpha}^{3D}|^2$) of the nth exciton,

$$|\phi_{n\alpha}^{3D}|^2 = \frac{V_0}{\pi (a_{B\alpha}^{3D})^3} n^3, \quad (8)$$

where $a_{B\alpha}^{3D}$ is the 3D-exciton Bohr radius and V_0 is the volume of the unit cell.

The contribution of the continuum excitons to $\varepsilon(E)$ is given by

$$\varepsilon(E) = \sum_{\alpha=A,B,C} \frac{A_{0x}^{C\alpha} E_{0\alpha}^{C1}}{4 G_{0\alpha}^{3D} (E + i\Gamma)^2} \ln \frac{(E_{0\alpha})^2}{(E_{0\alpha})^2 - (E + i\Gamma)^2}, \quad (9)$$

where $A_{0x}^{C\alpha}$ is the continuum-exciton strength parameter and $E_{0\alpha}^{C1}$ is the ground-state exciton energy ($\sim E_{0\alpha}$). The strength parameter $A_{0x}^{C\alpha}$ is proportional to the envelope function ($|\phi_k(0)|^2$) of the continuum-exciton state ($|k\rangle$),

$$|\phi_k(0)|^2 = \frac{\pi\alpha_k e^{\pi\alpha_k}}{N \sinh(\pi\alpha_k)} = \frac{2\pi\alpha_k}{N(1 - e^{\pi\alpha_k})}, \quad (10)$$

with

$$\alpha_k = \left| \frac{G_{0\alpha}^{3D}}{E - E_{0\alpha}} \right|^{1/2} = \left| \frac{G_{0\alpha}^{3D}}{(\hbar^2 \boldsymbol{k}^2 / 2\mu)} \right|^{1/2}. \quad (11)$$

In eqs. (10) and (11), N is the number of the unit cell in the crystal, μ is the exciton reduced mass, and $\boldsymbol{k}$ is the wave vector of the continuum exciton.

The fundamental reflectivity spectra of ZnO reveal the CPs at energies higher than 7 eV.[12–14] These CPs may correspond to transitions at several points (U, M, etc.) in the Brillouin zone and/or core exciton transitions. Since these transitions occur at energies well above our experimental range ($\leq$5 eV), we will not discuss these contributions to $\varepsilon(E)$.

3. Experimental

The ZnO single crystals used were purchased from the Fujitoku Corporation, Japan. They were grown by a vapor-phase method, not intentionally doped, and their surfaces were oriented parallel to the c axis. The crystals were mechanically polished with a diamond paste and degreased in organic solvents.

The automatic ellipsometer used was of the polarizer-sample-rotating-analyzer type (DVA-36VW-A, Mizojiri Optical, Co., Ltd., Japan). A 150 W xenon lamp was used as the light source. The SE data were obtained over the photon-energy range of 1.5–5.0 eV at room temperature. The angle of incidence and the polarizer azimuth were set at 70° and 20°, respectively.

Ellipsometry yields the complex ratio ρ between Fresnel's reflection coefficients r_p and r_s,[33]

$$\rho = \frac{r_s}{r_p} = \tan\psi e^{i\Delta}, \quad (12)$$

where Δ and ψ are the ellipsometric variables. At each photon energy $E = \hbar\omega$, the four optical parameters ($\varepsilon_{1\perp}$, $\varepsilon_{2\perp}$, $\varepsilon_{1/\!/}$, $\varepsilon_{2/\!/}$) can be determined from two pairs of SE measurements [ρ^{meas} ($\delta = 0°$ and $\delta = 90°$)] by minimizing the error function $G(\varepsilon_{1\perp}, \varepsilon_{2\perp}, \varepsilon_{1/\!/}, \varepsilon_{2/\!/})$,[25,26,29]

$$G(\varepsilon_{1\perp}, \varepsilon_{2\perp}, \varepsilon_{1/\!/}, \varepsilon_{2/\!/}) = \sum_{\delta=0°,90°} |\{\mathrm{Re}(\rho_\delta^{meas}) - \mathrm{Re}(\rho_\delta^{cal})\}^2 + \{\mathrm{Im}(\rho_\delta^{meas}) - \mathrm{Im}(\rho_\delta^{cal})\}^2|, \quad (13)$$

where ρ^{meas} ($\delta = 0°$ and $\delta = 90°$) are the reflection coefficients measured with that the c axis is parallel to both the interface and plane of incidence ($\delta = 0°$) or is parallel to the interface and perpendicular to the plane of incidence ($\delta = 90°$). ρ^{cal} is the calculated reflection co-

efficient ratio.

4. Results and Discussion

4.1 SE spectra

In Fig. 2 we show the pseudodielectric-function spectra of ZnO for both $\boldsymbol{E} \perp c$ and $\boldsymbol{E} /\!/ c$ measured by SE at room temperature (solid lines). Note that the pseudodielectric function is a quantity obtained from SE by means of the two-phase (ambient/substrate) model.[33] It is, thus, exactly equal to the true bulk dielectric function of a given sample if its surface is perfectly smooth and is film-free. Such an ideal condition can never be achieved in practice. Because neither the thickness nor the dielectric properties of the residual surface overlayer (oxide) are known, we did not attempt any correction for them. The SE data were also taken without correction for any surface roughness.

For comparison, the data obtained from the fundamental reflectivity by Freeouf[14] and those obtained from SE by Matz and Lüth[17] are plotted in Fig. 2 by the dashed and dotted lines, respectively. Klucker *et al.*[13] also obtained the dielectric-function spectra of ZnO from the reflectivity data by means of KK analysis. However, the ε_2 peak values obtained for both polarizations ($\sim$5) are much larger than those plotted in Fig. 2.

In Figs. 3 and 4 the pseudodielectric-function spectra of ZnO measured by us are shown by the solid circles. The main peaks in ε_2 (Fig. 4) at $\sim$3.4 eV for both $\boldsymbol{E} \perp c$ and $\boldsymbol{E} /\!/ c$ correspond to transitions at the fundamental absorption edge (E_0) of ZnO. The theoretical model given in Sec. II can be used to fit the experimental dispersion of $\varepsilon(E)$ over most of the spectral range. The parameters, such as $E_{0\alpha}$ and $A_{0\alpha}$ ($\alpha = A$, B and C), are commonly used as adjustable constants for the

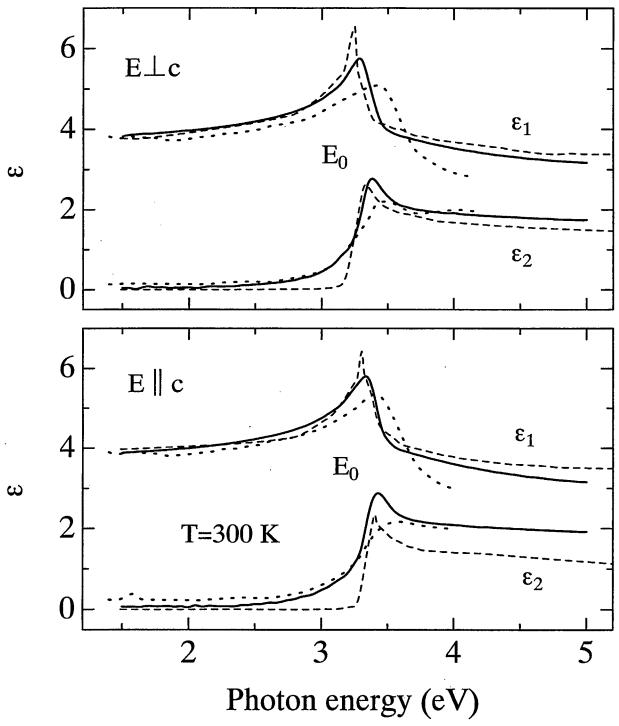

Fig. 2. Pseudodielectric-function spectra for ZnO measured by SE at room temperature (solid lines). For comparison, the fundamental-reflectivity data by Freeouf (ref. 14) and the SE data by Matz and Lüth (ref. 17) are also shown by the dashed and dotted lines, respectively.

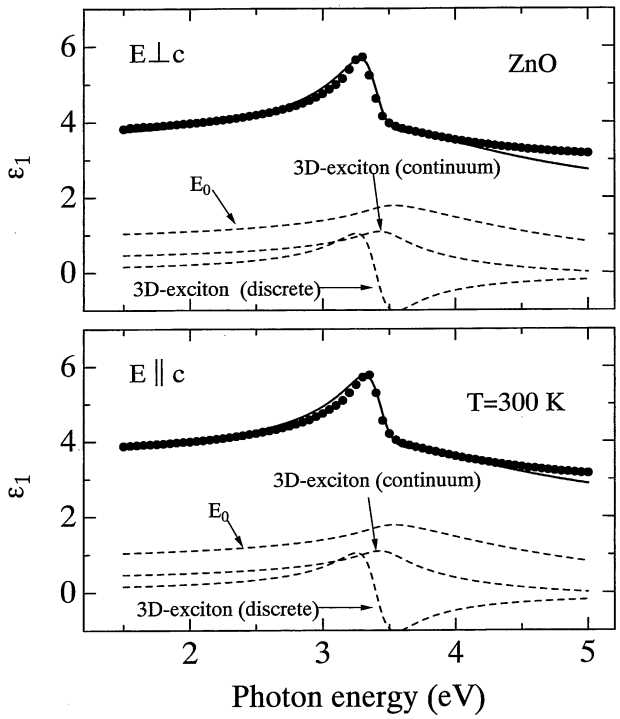

Fig. 3. $\varepsilon_1(E)$ spectrum for ZnO measured by SE at room temperature (solid circles). The solid lines represent the best-fitted results of our model to the experimental data. Individual contributions to $\varepsilon_1(E)$ of the various types of transitions are also shown by the dashed lines. They are obtained from eq. (2) for the one-electron contribution (E_0), from eq. (6) for the discrete-exciton contribution and from eq. (9) for the continuum-exciton contribution. The fit-determined CP parameters are listed in Table I.

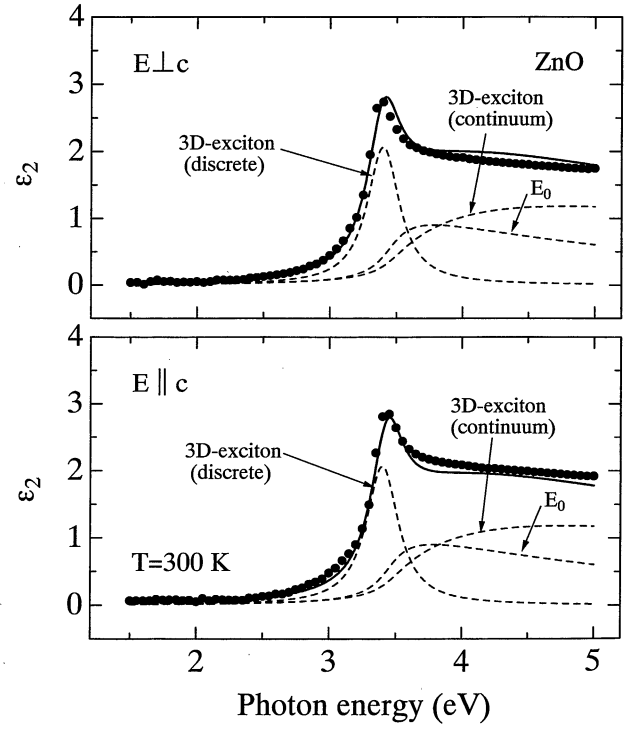

Fig. 4. As for Fig. 3, but for $\varepsilon_2(E)$.

Table I. Parameters used in the calculation of optical constants for ZnO.

Parameter	Polarization	
	$\boldsymbol{E} \perp c$	$\boldsymbol{E} /\!/ c$
E_{0A} (eV)	3.450	3.450
E_{0B} (eV)	3.453	
E_{0C} (eV)	3.484	3.484
$G_{0\alpha}^{3D}$ (meV)	59	59
A_{0A} (eV$^{1.5}$)	12.45	0.10
A_{0B} (eV$^{1.5}$)	12.50	
A_{0C} (eV$^{1.5}$)	0.05	24.90
A_{0x}^{1A} (eV)	0.13	0.001
A_{0x}^{1B} (eV)	0.13	
A_{0x}^{1C} (eV)	0.001	0.259
A_{0x}^{CA} (eV^2)	0.165	0.001
A_{0x}^{CB} (eV^2)	0.164	
A_{0x}^{CC} (eV^2)	0.006	0.329
$\Gamma(E_{0A})$ (eV)	0.145	0.145
$\Gamma(E_{0B})$ (eV)	0.145	
$\Gamma(E_{0C})$ (eV)	0.145	0.145
$\varepsilon_{1\infty}$	2.09	2.18

calculations of both ε_1 (=Reε) and ε_2 (=Imε). The experimental $\varepsilon_1(E)$ values are, however, usually somewhat larger than those obtained from our theoretical model. In order to improve the fit, therefore, we consider an additional term, $\varepsilon_{1\infty}$, to ε_1. This term is assumed to be constant and may arise from other higher-lying gaps and core exciton transitions.

The solid lines in Figs. 3 and 4 are obtained from the sum of eqs. (2), (6), (9) and $\varepsilon_{1\infty} = 2.09$ (2.18) for $\boldsymbol{E} \perp c$ ($\boldsymbol{E} /\!/ c$). The best-fit parameters are listed in Table I. Individual contributions to ε_1 and ε_2 of the various types of transitions are also shown in these figures by the dashed lines. They are obtained from eq. (2) for the one-electron contribution, from eq. (6) for the discrete-exciton contribution and from eq. (9) for the continuum-exciton contribution.

The E_0 CP is of the 3D M_0 type. Hence, the line shape of the corresponding one-electron $\varepsilon_2(E)$ spectrum [eq. (2)] is characterized by a continuous absorption obeying the well-known 1/2-power law, $\varepsilon_2 \propto (E-E_0)^{1/2}$. The excitonic states should, in principle, exist at each type of CP, since the Coulomb interaction is always present between the electrons and the holes. The 3D-exciton absorption spectrum consists of a series of sharp discrete lines with a rapidly decreasing oscillator strength $\propto n^{-3}$ [eq. (6)] and a continuum absorption due to the continuum (ionized) states [eq. (9)]. Recently, Mang *et al.*[34] determined the exciton Rydberg energies of $G_{0\alpha}^{3D}$ of ZnO using two-photon absorption spectroscopy to be $G_{0A}^{3D} = 63.1$ meV, $G_{0B}^{3D} = 50.4$ meV and $G_{0C}^{3D} = 48.9$ meV. For simplicity, however, we have assumed in the present analysis that $G_{0\alpha}^{3D} = 59$ meV ($\alpha = A, B, C$).[35]

It is understood from Fig. 4 that the continuum-exciton transitions at the E_0 edge [eq. (9)] behave like the one-electron characteristics [eq. (2)]. The deviations of the continuum-exciton spectrum from the one-electron spectrum are usually described by the so-called Sommerfeld or Coulomb enhancement factor.[36]

The lowest-direct band gap E_0 of the wurtzite crystals can be obtained from that of zinc-blende by the action of a small hexagonal crystal field.[37,38] Under the spin-orbit interaction, represented by the matrix element Δ_{so}, and that of the crystal field, represented by Δ_{cr}, the energy differences of the split-off valence bands are given by

$$E_{AB} = E_{0A} - E_{0B} = \frac{\Delta_{so} + \Delta_{cr}}{2} - \left[\left(\frac{\Delta_{so} + \Delta_{cr}}{2}\right)^2 - \frac{2}{3}\Delta_{so}\Delta_{cr}\right]^{1/2}, \quad (14.a)$$

$$E_{CB} = E_{0C} - E_{0B} = \frac{\Delta_{so} + \Delta_{cr}}{2} + \left[\left(\frac{\Delta_{so} + \Delta_{cr}}{2}\right)^2 - \frac{2}{3}\Delta_{so}\Delta_{cr}\right]^{1/2}. \quad (14.b)$$

The corresponding wave functions of the three valence bands are

$$|A\rangle : \quad \alpha_A S_- \uparrow + \alpha_C S_0 \downarrow, \quad (15.a)$$

$$|B\rangle : \quad S_+ \uparrow, \quad (15.b)$$

$$|C\rangle : \quad \alpha_C S_- \uparrow + \alpha_A S_0 \downarrow, \quad (15.c)$$

where $\uparrow$ and $\downarrow$ represent spin-up and spin-down, respectively, and S_+, S_- and S_0 are functions defined by the p-like basis functions. The admixture coefficients α_A and α_C are written as

$$\alpha_A = \left[1 + \frac{1}{2}\left(2 - \frac{3}{\Delta_{so}}E_{AB}\right)^2\right]^{-1/2}, \quad (16.a)$$

$$\alpha_C = \left[1 + \frac{1}{2}\left(2 - \frac{3}{\Delta_{so}}E_{CB}\right)^2\right]^{-1/2}, \quad (16.b)$$

where $\alpha_A^2 + \alpha_C^2 = 1$. Using the values listed in Table I, we obtain $\Delta_{so} = -15.0$ meV, $\Delta_{cr} = 35.5$ meV, $\alpha_A = 0.998$ and $\alpha_C = 0.063$. The energy parameters Δ_{so} and Δ_{cr} are comparable to those obtained by Mang *et al.* ($\Delta_{so} = -3.5$ meV and $\Delta_{cr} = 39.4$ meV at 6 K).[34]

The corresponding squared p-matrix elements $|\langle c|p|\nu\rangle|^2$ between the p-like valence and the s-like conduction band are

$$P_{0A\perp}^2 = \alpha_A^2(P^2/2), \quad P_{0B\perp}^2 = P^2/2, \quad P_{0A\perp}^2 = \alpha_C^2(P^2/2), \quad (17.a)$$

for $\boldsymbol{E} \perp c$, and

$$P_{0A/\!/}^2 = \alpha_C^2 P^2, \quad P_{0B/\!/}^2 = 0, \quad P_{0C/\!/}^2 = \alpha_A^2 P^2, \quad (17.b)$$

for $\boldsymbol{E} /\!/ c$. Then, we obtain the strength ratio

$$P_{0A\perp}^2 : P_{0B\perp}^2 : P_{0C\perp}^2 : P_{0A/\!/}^2 : P_{0B/\!/}^2 : P_{0C/\!/}^2 = 1.000 : 1.004 : 0.004 : 0.008 : 0 : 2.000. \quad (18)$$

The strength parameters, $A_{0\alpha}$ [eq. (3)], $A_{0x}^{n\alpha}$ [eq. (7)] and $A_{0x}^{C\alpha}$ [eq. (10)], are constrained to satisfy the above strength ratio of eq. (18) in the present analysis (see Table I). It is found that these parameters are in agreement with the experimental data (Figs. 3 and 4).

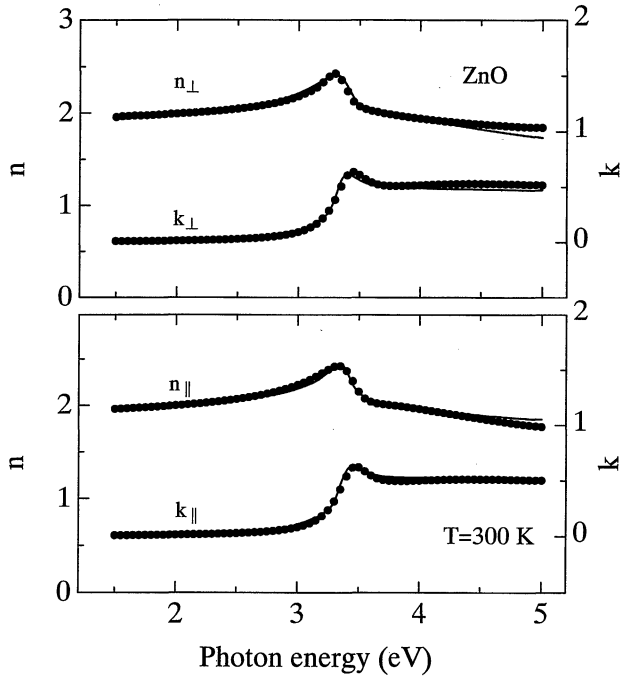

Fig. 5. Numerically calculated spectral dependence of the complex refractive index, $n^*(E) = n(E) + ik(E)$, for ZnO (solid lines). The solid circles represent the experimental data.

4.2 *Dielectric-function-related optical constants*

Optical constants, such as the complex refractive index $n^*(E) = n(E) + ik(E)$, absorption coefficient $\alpha(E)$ and normal-incidence reflectivity $R(E)$, can be easily obtained from the present study in the form of practical functions, since they are strongly related to the complex dielectric function, $\varepsilon(E)$.

The real refractive index $n(E)$ and extinction coefficient $k(E)$ can be written as

$$n(E) = \left(\frac{[\varepsilon_1(E)^2 + \varepsilon_2(E)^2]^{1/2} + \varepsilon_1(E)}{2} \right)^{1/2}, \quad (19)$$

$$k(E) = \left(\frac{[\varepsilon_1(E)^2 + \varepsilon_2(E)^2]^{1/2} - \varepsilon_1(E)}{2} \right)^{1/2}. \quad (20)$$

In Fig. 5 we show the numerically calculated spectral dependence of the complex refractive index, $n^*_\perp = n_\perp + ik_\perp (\boldsymbol{E} \perp c)$ and $n^*_{/\!/} = n_{/\!/} + ik_{/\!/} (\boldsymbol{E} /\!/ c)$, for ZnO (solid lines). They are obtained from eq. (19) for n and from eq. (20) for k. The solid circles represent the experimental data obtained by SE. The strong peaks in n and k at ~3.4 eV are mainly due to the discrete-exciton transitions.

The absorption coefficient $\alpha(E)$ and normal-incidence reflectivity $R(E)$ can be given by

$$\alpha(E) = \frac{4\pi}{\lambda} k(E), \quad (21)$$

$$R(E) = \frac{[n(E) - 1]^2 + k(E)^2}{[n(E) + 1]^2 + k(E)^2}, \quad (22)$$

where λ is the wavelength of light in vacuum.

The numerically calculated spectral dependence of α and R for ZnO are shown in Figs. 6 ($\boldsymbol{E} \perp c$) and 7 ($\boldsymbol{E} /\!/ c$) by the solid lines. The open and solid circles represent the SE data of α and R, respectively. It is seen in Figs. 6 and 7 that the reflectivity R shows the strong discrete-exciton peaks in the spectra. The absorption coefficients at these discrete-exciton peaks are ~2×10^5 cm^{-1} for both polarizations. Our calculated α and R spectra agree reasonably well with the experimental spectra.

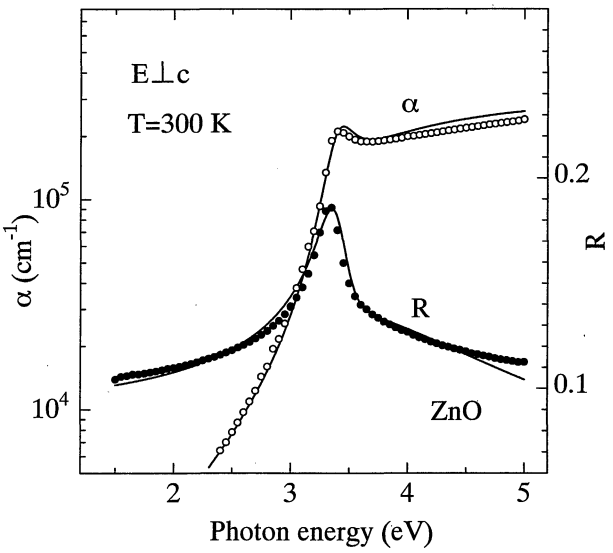

Fig. 6. Numerically calculated spectral dependence of the absorption coefficient $\alpha(E)$ and normal-incidence reflectivity $R(E)$ of ZnO for $\boldsymbol{E} \perp c$ (solid lines). The open and solid circles represent the experimental $\alpha(E)$ and $R(E)$, respectively.

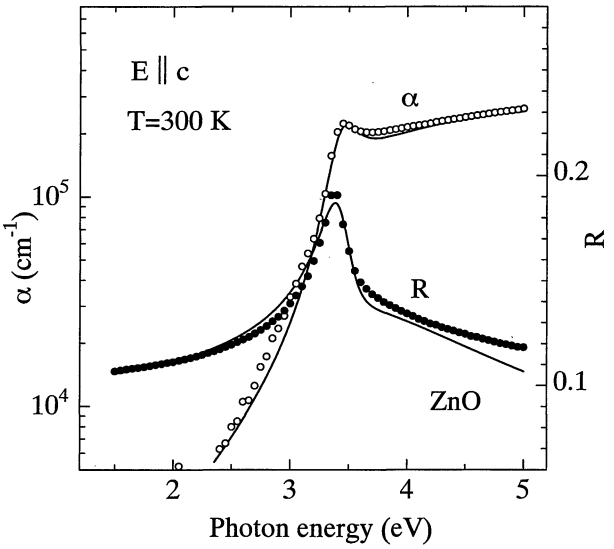

Fig. 7. As for Fig. 6, but for $\boldsymbol{E} /\!/ c$.

4.3 *Refractive-index dispersion in the transparent region*

It is important to know the refractive-index dispersion in the region below or near the fundamental absorption edge of semiconductors. Figures 8 and 9 show the experimental $n(E)$ dispersion of ZnO for $\boldsymbol{E} \perp c$ (Fig. 8) and $\boldsymbol{E} /\!/ c$ (Fig. 9) as measured using SE in the region near the discrete-exciton peaks. The open circles and open triangles represent the experimental data taken from the literature. They were obtained using the prism method

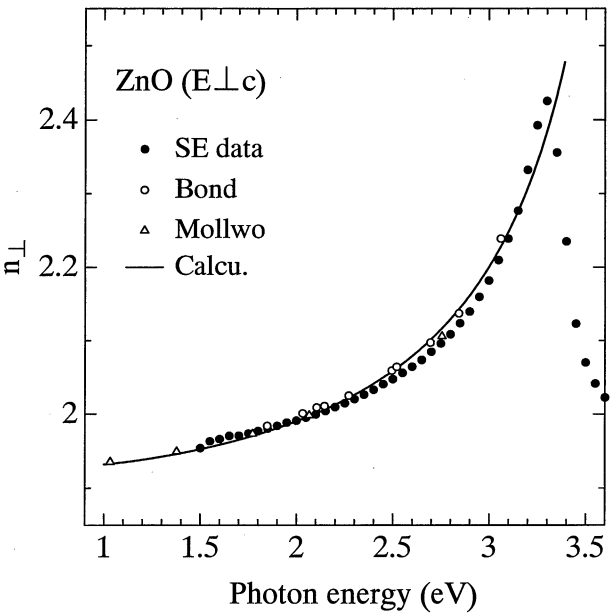

Fig. 8. Refractive-index dispersion of ZnO for $\boldsymbol{E} \perp c$ below the fundamental absorption edge. The solid circles represent our SE data. The open circles and open triangles represent the experimental data obtained by Bond (open circles, ref. 7) and Mollwo (open triangles, ref. 6), respectively.

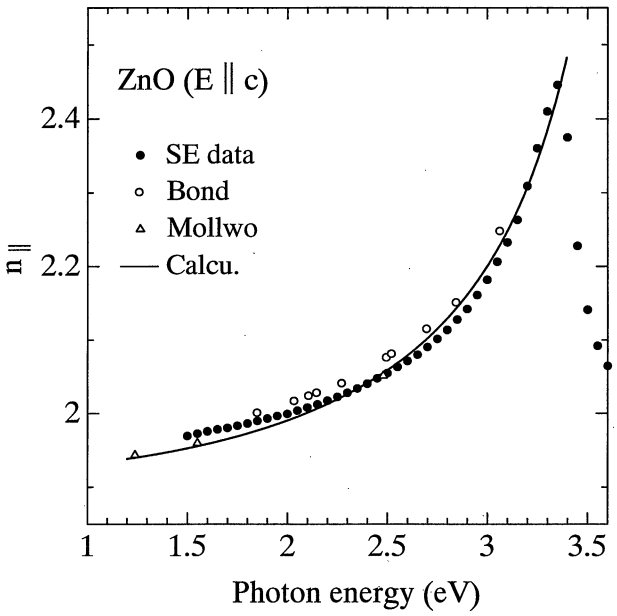

Fig. 9. As for Fig. 8, but for $\boldsymbol{E}/\!/c$.

by Bond (open circles)[7] and Mollwo (open triangles).[6]

The experimental $n(E)$ data in Figs. 8 and 9 are analyzed using the first-order Sellmeier equation:

$$n(\lambda)^2 = A + \frac{B\lambda^2}{\lambda^2 - C}, \tag{23}$$

where A, B and C are the fitting parameters and λ is in μm. The solid lines in Figs. 8 and 9 indicate the results of eq. (23) fitted to the experimental data. The values of the fitting parameters determined here are: $A = 2.84$, $B = 0.84$ and $C = 0.101\,\mu\text{m}^2$ ($\boldsymbol{E} \perp c$); $A = 2.85$, $B = 0.87$ and $C = 0.096\,\mu\text{m}^2$ ($\boldsymbol{E}/\!/c$).

As $\lambda \to \infty$, the electronic contribution to ε_1 approaches a limiting value ε_∞, the high-frequency dielectric constant. The ε_∞ value, which can be obtained from eq. (23) by $\varepsilon_\infty = n^2(\lambda \to \infty) = A + B$, are 3.68 for $\boldsymbol{E} \perp c$ and 3.72 for $\boldsymbol{E}/\!/c$. These values are in good agreement with those estimated by Heltemes and Swinney [$\varepsilon_\infty(\perp) = 3.70$ and $\varepsilon_\infty(/\!/) = 3.75$],[8] but are considerably smaller than those reported more recently by Venger *et al.* [$\varepsilon_\infty(\perp) = 3.95$ and $\varepsilon_\infty(/\!/) = 4.05$].[18]

Below the reststrahlen region, the real part of the dielectric function ε_1 approaches a limiting value, the static dielectric constant ε_s. ε_∞ and ε_s are related to the long-wavelength optical phonon frequencies, ω_{LO} and ω_{TO}, by the generalized Lyddane-Sachs-Teller relationship

$$\frac{\varepsilon_s}{\varepsilon_\infty} = \left(\frac{\omega_{LO}}{\omega_{TO}}\right)^2, \tag{24}$$

where ω_{LO} and ω_{TO} are the longitudinal and transverse optical phonon frequencies, respectively. Introducing $\omega_{LO} = 583\,\text{cm}^{-1}$ ($574\,\text{cm}^{-1}$), $\omega_{TO} = 411\,\text{cm}^{-1}$ ($380\,\text{cm}^{-1}$)[39] and $\varepsilon_\infty = 3.68$ (3.72) for $\boldsymbol{E} \perp c$ ($\boldsymbol{E}/\!/c$) into eq. (24), we obtain $\varepsilon_s = 7.40$ for $\boldsymbol{E} \perp c$ and 8.49 for $\boldsymbol{E}/\!/c$. These values are in reasonable agreement with those obtained by Heltemes and Swinney [$\varepsilon_s(\perp) = 7.8$ and $\varepsilon_s(/\!/) = 8.75$],[8] but are slightly smaller than the recent values obtained by Venger *et al.* [$\varepsilon_s(\perp) = 8.1$ and $\varepsilon_\infty(/\!/) = 9.0$].[18]

5. Conclusions

We have measured the spectral dependence of the complex dielectric function, $\varepsilon(E) = \varepsilon_1(E) + i\varepsilon_2(E)$, of ZnO for light polarized perpendicular ($\boldsymbol{E} \perp c$) and parallel to the optic axis c ($\boldsymbol{E}/\!/c$) using SE in the photon-energy range between 1.5 and 5.0 eV at room temperature. The measured SE spectra reveal the distinct structures at ~3.4 eV (E_0 edge). These $\varepsilon(E)$ spectra are analyzed on the basis of a simplified model of the interband transitions. Since the excitonic effects may modify the CP singularity structures, the model is made to account for the excitonic effects at this band edge. Our theoretical model successfully explains the experimental spectra over the entire range of photon energies. Dielectric-function-related optical constants, such as the complex refractive index ($n^* = n + ik$), absorption coefficient (α) and normal-incidence reflectivity (R), of ZnO are also presented. The refractive-index data in the transparent region of ZnO have also been analyzed using the first-order Sellmeier equation. As a byproduct, the high-frequency and static dielectric constants are determined as $\varepsilon_\infty = 3.68$ and $\varepsilon_s = 7.40$ for $\boldsymbol{E} \perp c$ and $\varepsilon_\infty = 3.72$ and $\varepsilon_s = 8.49$ for $\boldsymbol{E}/\!/c$.

Acknowledgement

We would like to thank Dr. T. Miyazaki for his kind advice concerning this work.

1) *Numerical Data and Functional Relationships in Science and Technology*, eds. K.-H. Hellwege and O. Madelung (Springer, Berlin, 1982) Landolt-Bnstein, New Series, Group III, Vol. 17, Pt. a.
2) J. A. Aranovich, D. Golmayo, A. L. Fahrenbruch and R. H.

Bube: J. Appl. Phys. **51** (1980) 4260.
3) S. Pizzini, N. Butta, D. Narducci and M. Palladino: J. Electrochem. Soc. **136** (1989) 1945.
4) F. S. Hickernell: Proc. IEEE **64** (1976) 631.
5) T. Shiosaki, N. Kitamura and A. Kawabata: Proc. IEEE Ultrasonics Symp. (1991) p. 296.
6) E. Mollwo: Z. Angew. Phys. **6** (1954) 257.
7) W. L. Bond: J. Appl. Phys. **36** (1965) 1674.
8) E. C. Heltemes and H. L. Swinney: J. Appl. Phys. **38** (1967) 2387.
9) Y. S. Park, C. W. Litton, T. C. Collins and D. C. Reynolds: Phys. Rev. **143** (1966) 512.
10) W. Y. Liang and A. D. Yoffe: Phys. Rev. Lett. **20** (1968) 59.
11) Y. S. Park and J. R. Schneider: J. Appl. Phys. **39** (1968) 3049.
12) R. L. Hengehold, R. J. Almassy and F. L. Pedrotti: Phys. Rev. B **1** (1970) 4784.
13) R. Klucker, H. Neelkowski, Y. S. Park, M. Skibowski and T. S. Wagner: Phys. Status Solidi B **45** (1971) 265.
14) J. L. Freeouf: Phys. Rev. B **7** (1973) 3810.
15) K. Hmer: Phys. Status Solidi B **56** (1973) 249.
16) K. Hümmer and P. Gebhardt: Phys. Status Solidi B **85** (1978) 271.
17) R. Matz and H. Lh: Appl. Phys. **18** (1979) 123.
18) E. F. Venger, A. V. Melnichuk, L. Yu. Melnichuk and Yu. A. Pasechnik: Phys. Status Solidi B **188** (1995) 823.
19) S. Zollner, M. Garriga, J. Humlek, S. Gopalan and M. Cardona: Phys. Rev. B **43** (1991) 4349.
20) U. Rossow: *Optical Characterization of Epitaxial Semiconductor Layers*, eds. G. Bauer and W. Richter (Springer-Verlag, Berlin, 1996) p. 68.
21) F. Meyer, E. E. de Kluizenaar and D. den Engelsen: J. Opt. Soc. Am. **63** (1973) 529.
22) D. E. Aspnes, J. C. Phillips, K. L. Tai and P. M. Bridenbaugh: Phys. Rev. B **23** (1981) 816.
23) S. Logothetidis, L. Viña and M. Cardona: Phys. Rev. B **31** (1985) 2180.
24) S. Logothetidis, P. Lautenschlager and M. Cardona: Phys. Rev. B **33** (1986) 1110.
25) S. Logothetidis, M. Cardona, P. Lautenschlager and M. Garriga: Phys. Rev. B **34** (1986) 2458.
26) S. Ninomiya and S. Adachi: J. Appl. Phys. **78** (1995) 4681.
27) S. Logothetidis and H. M. Polatoglou: Phys. Rev. B **36** (1987) 7491.
28) A. K. Harman, S. Ninomiya and S. Adachi: J. Appl. Phys. **76** (1994) 8032.
29) S. Ninomiya and S. Adachi: J. Appl. Phys. **78** (1995) 1183.
30) The group-theoretical symbols used here are taken from G. F. Koster, J. O. Dimmock, R. G. Wheeler and H. Statz: *Properties of Thirty-Two Point Groups* (MIT Press, Cambridge, 1963).
31) S. Adachi: *GaAs and Related Materials: Bulk Semiconducting and Superlattice Properties* (World Scientific, Singapore, 1994).
32) R. J. Elliott: Phys. Rev. **108** (1957) 1384.
33) R. M. A. Azzam and N. M. Bashara: *Ellipsometry and Polarized Light* (North-Holland, Amsterdam, 1977).
34) A. Mang, K. Reimann and St. Renacke: Solid State Commun. **94** (1995) 251.
35) D. C. Reynolds and T. C. Collins: *Excitons, Their Properties and Uses* (Academic, New York, 1981).
36) See, for instance, H. Haug and S. W. Koch: *Quantum Theory of the Optical and Electronic Properties of Semiconductors* (World Scientific, Singapore, 1993).
37) D. G. Thomas and J. J. Hopfield: Phys. Rev. **116** (1959) 573.
38) J. J. Hopfield: J. Phys. Chem. Solids **15** (1960) 97.
39) T. C. Damen, S. P. S. Porto and B. Tell: Phys. Rev. **142** (1966) 570.